

Large Chern numbers in a dissipative dice model

Shujie Cheng¹ and Gao Xianlong¹

¹*Department of Physics, Zhejiang Normal University, Jinhua 321004, China*

(Dated: December 8, 2021)

For decades, the topological phenomena in quantum systems have always been catching our attention. Recently, there are many interests on the systems where topologically protected edge states exist, even in the presence of non-Hermiticity. Motivated by these researches, the topological properties of a non-Hermitian dice model are studied in two non-Hermitian cases, viz. in the imbalanced and the balanced dissipations. Our results suggest that the topological phases are protected by the real gaps and the bulk-edge correspondence readily seen in the real edge-state spectra. Besides, we show that the principle of the bulk-edge correspondence in Hermitian case is still effective in analyzing the three-band non-Hermitian system. We find that there are topological non-trivial phases with large Chern numbers $C = -3$ robust against the dissipative perturbations.

I. INTRODUCTION

Topology acts as a critical role in physics, and the topological phenomena have attracted increasing interests in the fields of the topological condensed matters [1, 2], topological photonics systems [3, 4], and the ultra-cold atomic systems [5–7], in which the characterization of topological properties is out of the framework of spontaneous symmetry breaking [8, 9]. Besides, due to the symmetries, the topological classification of Hermitian systems was well established [10, 11]. A typical signature of topology is the bulk-edge correspondence, which typically gives the relationships between the topological invariants and the associated edge states [12, 13] and makes insulators [1, 14–20] and superconductors [2, 21–23] fantastic and applicable.

Beyond the investigated topological phenomena in Hermitian systems, there are great attention on the framework of the open systems, in which the energy or particles are no longer conserved [24, 25]. Generally speaking, open systems are also interpreted as the non-Hermitian systems described by the effective non-Hermitian Hamiltonians. Recent years there are plenty of progress made in theoretical [26–57] and experimental [58–66] researches in revealing the topological nature of the systems in the presence of non-Hermiticity. Different from the Hermitian systems, it was studied that there were 38-fold symmetries in the non-Hermitian case [38], leading to the well-established topological classification of the non-Hermitian systems.

Similar to the Hermitian case, the bulk-edge correspondence remains a central topic in the non-Hermitian cases. However, there is a subtle issue on how the bulk-edge correspondence exists. Previous works show that the bulk-edge correspondence maintains by the Bloch topological invariants [31–36] in the presence of the non-Hermiticity. Moreover, the non-Hermiticity can lead to anomalous edge states [37]. Furthermore, the non-Hermiticity can be induced by the imbalanced tunnelings, leading to the non-Hermitian skin effect [40, 41]. In such a system, the

conventional bulk-edge correspondence is altered and replaced by the generalized bulk-edge correspondence suggested by the non-Bloch band theory [40, 41].

Combined with the recent researches on Dice models [67–69], in which large Chern numbers and multiple edge states are uncovered, in this paper, we are motivated to study the topological properties of a dissipative non-Hermitian Dice model. To be concrete, we make attempt to answer the questions whether large Chern numbers are robust against the dissipative perturbations and how the bulk-edge correspondence exists.

The rest of paper are organized as follows. Section II describes our general non-Hermitian model. Section III briefly makes a definition of the Chern numbers of the non-Hermitian systems and specifies two Chern markers to characterize the topological properties of systems. Section IV involves the analyses and discussions of two typically dissipative cases. Finally, we make a conclusion in Sec. V.

II. MODEL AND HAMILTONIAN

In this paper, we study a non-interacting model with dissipative on-site potentials based on a dice lattice [70–74], shown in Fig. 1. Intuitively, there are three non-equivalent sublattice sites, marked as R (red dots), B (blue dots), and G (green dots). Thus the lattice model belongs to the SU(3) system [67–69, 75, 76]. The single-particle Hamiltonian consists of the following two parts,

$$\hat{H} = \hat{H}_1 + \hat{H}_2. \quad (1)$$

\hat{H}_1 denotes the Hermitian part, which has been pro-

posed in Ref. [68] with

$$\begin{aligned} \hat{H}_1 = & \left[\sum_{\langle \mathbf{R}_i, \mathbf{B}_j \rangle} t \hat{c}_{\mathbf{R}_i}^\dagger \hat{c}_{\mathbf{B}_j} + \sum_{\langle \mathbf{R}_i, \mathbf{G}_\ell \rangle} t_1 \hat{c}_{\mathbf{R}_i}^\dagger \hat{c}_{\mathbf{G}_\ell} \right. \\ & + \sum_{\langle \mathbf{B}_j, \mathbf{G}_\ell \rangle} t_1 \hat{c}_{\mathbf{B}_j}^\dagger \hat{c}_{\mathbf{G}_\ell} + \sum_{\langle \mathbf{R}_i, \mathbf{R}_j \rangle} t_2 e^{i\phi} \hat{c}_{\mathbf{R}_i}^\dagger \hat{c}_{\mathbf{R}_j} \\ & \left. + \sum_{\langle \mathbf{B}_i, \mathbf{B}_j \rangle} t_2 e^{i\phi} \hat{c}_{\mathbf{B}_i}^\dagger \hat{c}_{\mathbf{B}_j} + H.c. \right] + \gamma_1 \Delta \sum_{\mathbf{R}_i} \hat{c}_{\mathbf{R}_i}^\dagger \hat{c}_{\mathbf{R}_i} \\ & + \gamma_1 \Delta \sum_{\mathbf{B}_i} \hat{c}_{\mathbf{B}_i}^\dagger \hat{c}_{\mathbf{B}_i} + \gamma_2 \Delta \sum_{\mathbf{G}_i} \hat{c}_{\mathbf{G}_i}^\dagger \hat{c}_{\mathbf{G}_i}, \end{aligned} \quad (2)$$

in which t is the hopping amplitude between one R site and one B site, t_1 is the hopping amplitude between one G site and one R or B site, $t_2 e^{-i\phi}$ is the complex tunneling amplitude of the next-nearest-neighbor tunnelings between the same adjacent sublattices with ϕ being the phase, and $\gamma_1 \Delta$ and $\gamma_2 \Delta$ denote strengths of on-site potentials with Δ being the modulation parameter and γ_1 and γ_2 the modulation rate of Δ .

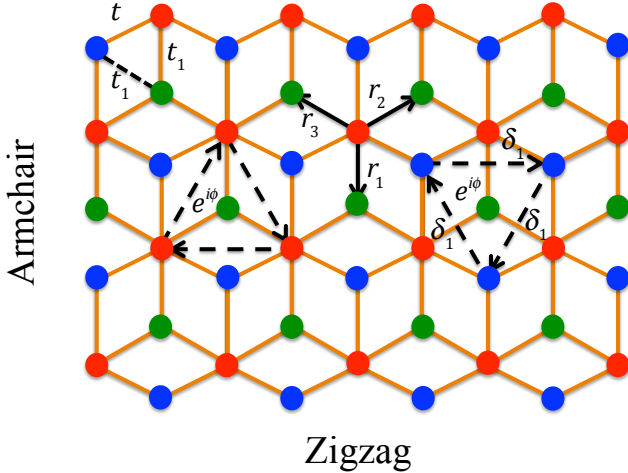


Figure 1: The sketch of dice lattice formed by staggered arrangement of sublattice R (red), B (blue), and G (green). The Hamiltonian \hat{H} consists of the nearest neighbor tunnelings with hopping amplitude t between one R site and one B site, and t_1 between one G site and one R or B site, and the phase-dependent next-nearest-neighbor tunnelings with hopping amplitude $t_2 e^{i\phi}$ between the same R or B sublattice sites. Moreover, each lattice site is subject to the potentials and dissipations. The vectors \mathbf{r}_s ($s=1,2,3$) point from the centering site to its neighboring sites and the vectors δ_s ($s=1,2,3$) connect the next-nearest-neighbor R or B sites. Zigzag and armchair are two common geometric boundary shapes, which will be used for the discussions of the bulk-edge correspondence.

\hat{H}_2 represents the non-Hermitian part which shows that each sublattice is attached with dissipation, and is proposed as

$$\hat{H}_2 = i\eta \sum_{\mathbf{R}_i} \hat{c}_{\mathbf{R}_i}^\dagger \hat{c}_{\mathbf{R}_i} + i\eta \sum_{\mathbf{B}_i} \hat{c}_{\mathbf{B}_i}^\dagger \hat{c}_{\mathbf{B}_i} + i\chi\eta_1 \sum_{\mathbf{G}_i} \hat{c}_{\mathbf{G}_i}^\dagger \hat{c}_{\mathbf{G}_i}, \quad (3)$$

where η and η_1 are the strengths of the dissipations with the same sign, and $\chi \in \pm 1$ plays the role of a switch by weighing overall gain and loss of the system. When $\eta = \eta_1 = 0$, the system becomes the Hermitian dice model [68], and if the tunnelings between G sites and B sites are omitted, then it goes back to the Haldane-like Dice model [69].

Under the discrete translational symmetry, the Hamiltonian \hat{H}_1 can be mapped into momentum space by using the discrete Fourier transformation

$$\hat{c}_{\mathbf{k},\alpha} = \frac{1}{\sqrt{N}} \sum_{\alpha_j} e^{-i\mathbf{k} \cdot \alpha_j} \hat{c}_{\alpha_j}, \quad (4)$$

where N is the total number of the unit cells, and $\alpha \in \{\mathbf{R}, \mathbf{B}, \mathbf{G}\}$ denotes the type of sublattice with α_j being the corresponding coordinate. Thus, the Bloch Hamiltonian has a form as

$$\hat{H}(\mathbf{k}) = \sum_{\mathbf{k}} \hat{c}_{\mathbf{k}}^\dagger \hat{\mathcal{H}}(\mathbf{k}) \hat{c}_{\mathbf{k}}, \quad (5)$$

where $\hat{c}_{\mathbf{k}}^\dagger = (\hat{c}_{\mathbf{k},\mathbf{R}}, \hat{c}_{\mathbf{k},\mathbf{B}}, \hat{c}_{\mathbf{k},\mathbf{G}})^T$ is the three-component basis, and $\mathcal{H}(k)$ is expressed as

$$\mathcal{H}_{\mathbf{k}} = I(\mathbf{k}, \eta, \eta_1) + \mathbf{d}(\mathbf{k}) \cdot \vec{\lambda}, \quad (6)$$

where $I(\mathbf{k}, \eta, \eta_1)$ is the scalar leading to a overall shift of the energy in a complex space, $\mathbf{d}(\mathbf{k})$ is a coefficient vector, and $\vec{\lambda}$ is a vector consisting of the Gell-Mann matrices [68, 75, 76]. Concretely, the components of $\mathbf{d}(\mathbf{k})$ are displayed as

$$\begin{aligned} d_1 &= t \sum_s \cos(\mathbf{k} \cdot \mathbf{r}_s), \quad d_2 = t \sum_s \sin(\mathbf{k} \cdot \mathbf{r}_s), \\ d_4 &= d_6 = t_1 \sum_s \cos(\mathbf{k} \cdot \mathbf{r}_s), \\ d_7 &= -d_5 = t_1 \sum_s \sin(\mathbf{k} \cdot \mathbf{r}_s), \\ d_3 &= -2t_2 \sin \phi \sum_s \sin(\mathbf{k} \cdot \delta_s) + \frac{i\eta}{3}, \\ d_8 &= \frac{\gamma_1 - \gamma_2}{\sqrt{3}} \Delta + \frac{2t_2}{\sqrt{3}} \cos \phi \sum_s \cos(\mathbf{k} \cdot \delta_s) + \frac{i(2\eta - \chi\eta_1)}{\sqrt{3}}, \end{aligned} \quad (7)$$

with six vectors \mathbf{r}_s and δ_s ($s=1,2,3$) being expressed as

$$\begin{aligned} \mathbf{r}_1 &= \begin{pmatrix} 0 \\ -1 \end{pmatrix}, \quad \mathbf{r}_2 = \frac{1}{2} \begin{pmatrix} \sqrt{3} \\ 1 \end{pmatrix}, \quad \mathbf{r}_3 = \frac{1}{2} \begin{pmatrix} -\sqrt{3} \\ 1 \end{pmatrix}, \\ \delta_1 &= \begin{pmatrix} \sqrt{3} \\ 0 \end{pmatrix}, \quad \delta_2 = \frac{1}{2} \begin{pmatrix} -\sqrt{3} \\ 3 \end{pmatrix}, \quad \delta_3 = -\frac{1}{2} \begin{pmatrix} \sqrt{3} \\ 3 \end{pmatrix}. \end{aligned} \quad (8)$$

III. CHERN NUMBERS

According to the 38-fold topological classification for the non-Hermitian systems, our systems under research belong to the A class in complex Altland-Zirnbauer symmetry [38]. In this section, we briefly describe how to define the Chern numbers of associated energy bands of our systems. To begin with, we discuss the eigenstates of the non-Hermitian systems. Compared with the Hermitian systems, the eigenstates in the non-Hermitian systems form the biorthogonal bases [39], which satisfy

$$\begin{aligned}\mathcal{H}_{\mathbf{k}}|\psi_n^R\rangle &= E_n|\psi_n^R\rangle, \\ \mathcal{H}_{\mathbf{k}}^\dagger|\psi_n^L\rangle &= E_n^*|\psi_n^L\rangle,\end{aligned}\quad (9)$$

where $|\psi_n^R\rangle$ denotes the right eigenstate of $\mathcal{H}_{\mathbf{k}}$ and $|\psi_n^L\rangle$ is the left eigenstate. We define the bottom band, middle band and top band according to the real eigenvalues of $\mathcal{H}_{\mathbf{k}}$, and the ascending value of n ($n = 1, 2, 3$) corresponds to the three bands from bottom to top. Furthermore, the biorthogonal bases obey such a biorthogonality relation

$$\langle\psi_{n'}^R|\psi_n^L\rangle = \langle\psi_{n'}^L|\psi_n^R\rangle = \delta_{n'n}, \quad (10)$$

and fulfill the completeness condition

$$\sum_n |\psi_n^L\rangle \langle\psi_n^R| = \sum_n |\psi_n^R\rangle \langle\psi_n^L| = I. \quad (11)$$

With these definitions, the \mathbb{Z} topological invariant, namely the Chern number is defined as [40, 44–46]

$$C_n = \frac{1}{2\pi} \int_{\text{1st BZ}} \Omega_n(\mathbf{k}) d^2\mathbf{k}, \quad (12)$$

in which $\Omega_n(\mathbf{k}) = \partial_{k_x} A_n^y(\mathbf{k}) - \partial_{k_y} A_n^x(\mathbf{k})$ denotes the Berry curvature of the n th band and $A_n^j(\mathbf{k}) = i \langle\psi_n^L(\mathbf{k})|\partial_{k_j}\psi_n^R(\mathbf{k})\rangle$ ($j = x, y$) is the Berry connection, obtained from the non-Hermitian Hamiltonian. Hereinbelow, for convenience, we will use two Chern markers, namely $C_{\frac{1}{3}} = C_1$ and $C_{\frac{2}{3}} = C_1 + C_2$ to characterize the topological phases of the non-Hermitian systems.

IV. RESULTS AND DISCUSSIONS

In this section, two non-Hermitian cases will be investigated, i.e., the imbalanced dissipation and the balanced dissipation, respectively. The imbalanced dissipation denotes that the overall gain and loss are not conserved and the balanced dissipation refers to the case where the gain and loss are balanced. Without loss of generality, we fix t as the unit of energy and set some other global parameters with $t_1 = 0.5t$, $t_2 = 0.526t$, $\phi = \frac{\pi}{2}$, $\gamma_1 = 5$, and $\gamma_2 = 7$. The following main effort is focused on the investigation in the large Chern numbers and the bulk-edge correspondence with the existence of dissipations.

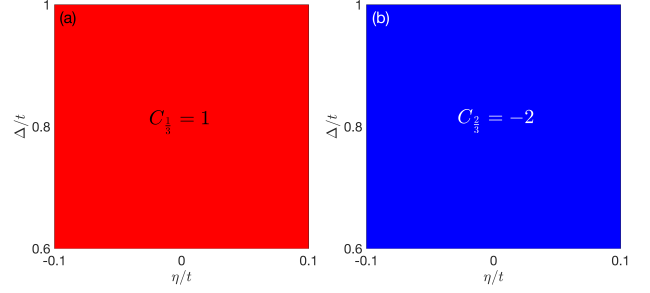


Figure 2: Two phase diagrams in the Δ - η parameter space. (a) $C_{\frac{1}{3}} = 1$. There is a topological non-trivial bottom band with Chern number $C_1 = C_{\frac{1}{3}} = 1$. (b) $C_{\frac{2}{3}} = -2$. There is a topological non-trivial middle band with large Chern number $C_2 = C_{\frac{2}{3}} - C_{\frac{1}{3}} = -3$. The involved parameters are $\Delta \in [0.6t, 1t]$, $\eta = \eta_1 \in [-0.1t, 0.1t]$, and $\chi = 1$.

A. Imbalanced dissipation

By taking $\eta_1 = 2\eta$ ($\eta \in [-0.1t, 0.1t]$) and $\chi = 1$, the overall gain and loss are not conserved. Furthermore, the value of η determines whether the non-Hermitian potential is pure gain or loss type. And as a result, the system belongs to the imbalanced dissipation case. With these matrix elements in Eq. (7), we calculate the Chern numbers by means of the definition in Eq. (12) and two phase diagrams are plotted in Figs. 2(a) and 2(b), respectively. From Fig. 2(a), we know that in the chosen parameter region, the bottom band of system is topological nontrivial with Chern number $C_1 = C_{\frac{1}{3}} = 1$. From Fig. 2(b), we intuitively notice that there is a large Chern number of the middle band of the system. Through a simple mathematical relationship, the middle band has a large Chern number with $C_2 = C_{\frac{2}{3}} - C_1 = -3$. In addition, the topological properties of bands are protected by real gaps [31, 32]. To check this point, we then choose three parameter points $(\eta_a, \Delta_a) = (-0.1t, 0.6t)$, $(\eta_b, \Delta_b) = (0.1t, 0.8t)$, and $(\eta_c, \Delta_c) = (0.1t, 1t)$ in the phase diagram. We here point out that we have tested that the parameter interval supporting non-zero Chern number is relatively large, which is quite beneficial to make use of the topological properties of the system. However, when the dissipation strength further increases, the real energy spectra becomes gapless, leading to the result that fails to define an effective Chern number [40, 44–46]. We here in the paper concentrate on the cases with the dissipation strength where the real energy spectra are gapped.

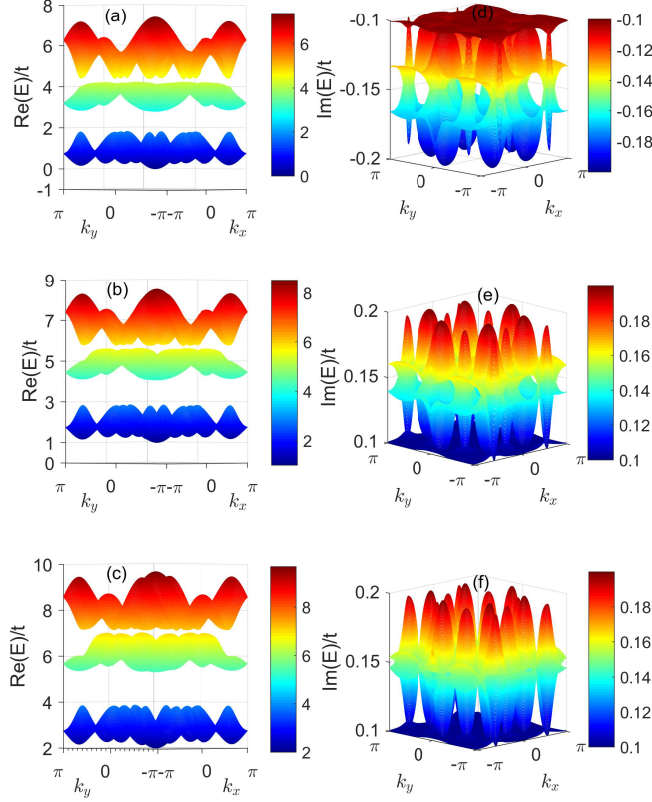


Figure 3: Energy spectra at the chosen parameter points in the imbalanced dissipation case. Top panel: energy spectra at (η_a, Δ_a) , with the real part in (a) and the imaginary part in (d). Middle panel: energy spectra at (η_b, Δ_b) , with the real part in (b) and the imaginary part in (e). Bottom panel: energy spectra at (η_c, Δ_c) , with the real part in (c) and the imaginary part in (f). Intuitively, the bands in (a), (b) and (c) are isolated, whereas the energies in the imaginary part are continuous.

Figures. 3(a)-3(f) are the energy spectra at these chosen parameter points with Figs. 3(a), 3(b), and 3(c) being the real spectra and Figs. 3(d), 3(e), and 3(f) being the corresponding imaginary spectra. We notice that all the real spectra have separated bands, whereas the imaginary parts are continuous. This phenomenon means the topological property of energy bands in the imbalanced dissipation case is associated with the real gaps [31, 32].

Further, we consider a semi-infinite cylindrical geometries with a zigzag edge to discuss the bulk-edge correspondence, and the shape of geometry keeps the same as that in previous works [68]. To be precise, we take $N_{\text{zigzag}} = 86$ which corresponds to the number of the lattice sites contained in the periodic repeating cell of the zigzag edge case. With the method of partial Fourier transformation utilized in Ref. [68], by choosing the parameter point (η_c, Δ_c) mentioned in this subsection before, we obtain the edge-state spectra as a function of k_x ,

shown in Figs. 4(a) and 4(b), respectively.

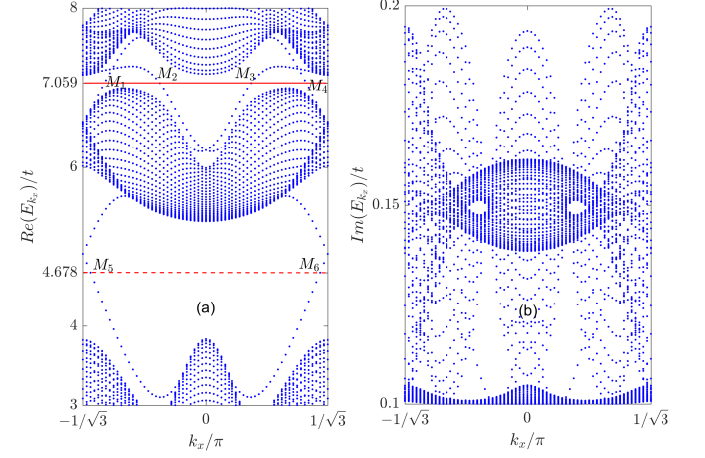


Figure 4: Edge-state spectra with the zigzag edge at the chosen parameter point (η_c, Δ_c) (parts of the lower and higher $\text{Re}(E_{k_x})$ are not shown). The bulk-edge correspondence is readily seen in the real spectrum. (a) The real edge-state spectrum. Obviously, there are two pairs of edge modes within the upper bulk gap and a pair of edge modes within the lower bulk gap, corresponding to $C_{\frac{2}{3}} = -2$ and $C_{\frac{1}{3}} = 1$, respectively. Four edge modes, labeled as M_1 , M_4 , M_2 and M_3 are chosen at $\text{Re}(E_{k_x}) = 7.059t$ (red solid line) and a pair of edge modes, labeled as M_5 and M_6 are chosen at $\text{Re}(E_{k_x}) = 4.678t$ (red dashed line). (b) The imaginary part of the edge-state spectrum. Different from the real part in (a), this imaginary edge-state spectrum is continuous, although there is a certain broadening. Meanwhile, no obvious bulk-edge correspondence phenomenon occurs in the imaginary part. Other involved parameter is $N_{\text{zigzag}} = 86$, and the number of discrete k_x is 65.

Figure 4(a) is the real edge-state spectrum in the zigzag edge case, where there are two pairs of edge modes within the upper bulk gap and a pair of edge modes within the lower bulk gap, which can be reflected from the phase diagrams in Figs. 2(a) and 2(b), showing the bulk-edge correspondence. Besides, from the edge-state spectra, it is shown that the edge states are protected by the real gaps, which is consistent with the analyses of the energy spectra in Figs. 3(c) and 3(f). M_1 and M_4 and M_2 and M_3 are two pairs of edge modes chosen at $\text{Re}(E_{k_x}) = 7.059t$ (red solid line) and M_5 and M_6 are a pair of edge modes chosen at $\text{Re}(E_{k_x}) = 4.678t$ (red dashed line). As for the imaginary edge-state spectrum in Fig. 4(b), the energies are continuous, and there is no obvious bulk-edge correspondence in it.

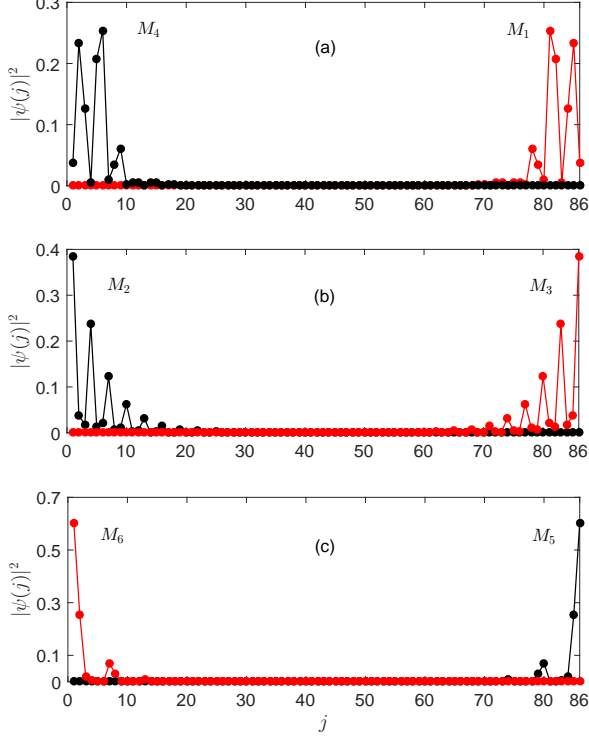


Figure 5: The spatial density distributions of the six chosen edge modes M_1 - M_6 . Edge modes with a positive group velocity are shown in red, whereas those with a negative group velocity are shown in black, presenting the chiral symmetry. j is the site index.

In order to further understand the bulk-edge correspondence, we plot the spatial density distributions of the six chosen edge modes M_1 - M_6 of the zigzag edge case, which are shown in Fig. 5. We conclude that the edge modes appear in pairs with opposite momentums. Besides, the edge modes with positive group velocity are shown in red, whereas those with negative group velocity are shown in black, presenting the chiral symmetry. We emphasize that the discussion of the spatial density distributions of the edge modes in the armchair edge case [68] will yield similar results, which will not be analysed here any more. We find that the principle of bulk-edge correspondence mentioned in Ref. [13] is still effective in the non-Hermitian case. Similar to its applications in Ref. [68], we focus on the edge modes localized at the $j = 1$ side to discuss the relationship between the bulk Chern number and the edge states. According to the phase diagram in Fig. 2(a), we know that the edge modes M_6 carries the Chern number $C = 1$, and the edge modes M_2 and M_4 with an opposite group velocity both of the Chern number $C = -1$. Hence, the Chern number of the middle band is $C_2 = -1 + (-1) - 1 = -3$ which is self-consistent with the phase diagrams.

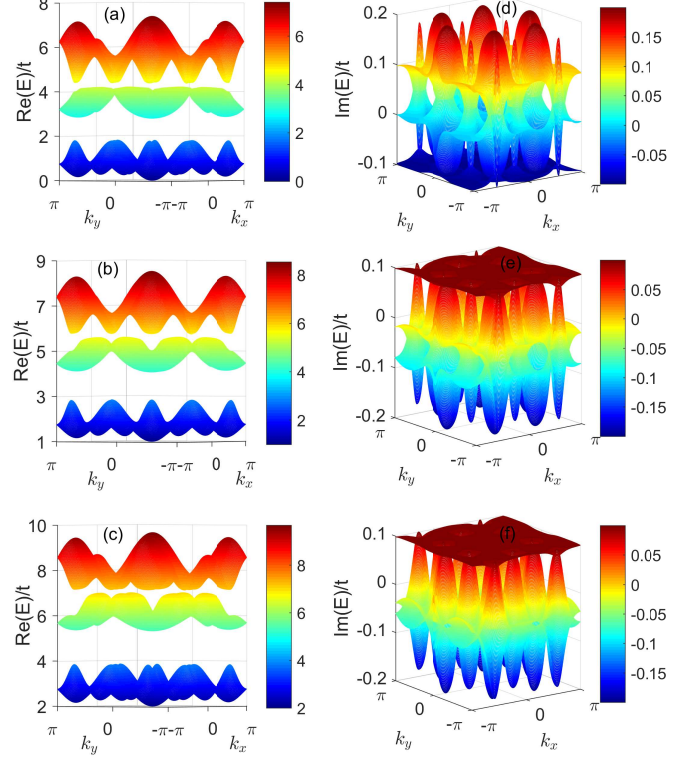


Figure 6: Energy spectra at the chosen parameter points in the balanced dissipation case. Top panel: energy spectra at (η_a, Δ_a) , with the real part in (a) and the imaginary part in (d). Middle panel: energy spectra at (η_b, Δ_b) , with the real part in (b) and the imaginary part in (e). Bottom panel: energy spectra at (η_c, Δ_c) , with the real part in (c) and the imaginary part in (f). Intuitively, the imaginary parts of energy spectra show an obvious broadening and continuous band without separation. Instead, the bands in the real part are all clearly separated.

B. Balanced dissipation

A non-Hermitian system with balanced dissipations means a balanced gain and loss. For the purpose of studying topological properties of such a non-Hermitian with balanced dissipations, we specify $\chi = -1$ and $\eta_1 = 2\eta$ with $\eta \in [-0.1t, 0.1t]$. Then we substitute these parameters in Eq. (7) into the definition of Chern number and uncover that the obtained phase diagrams are consistent with the imbalanced dissipative system. Our numerical results show that the large Chern number is still robust in the balanced dissipation case.

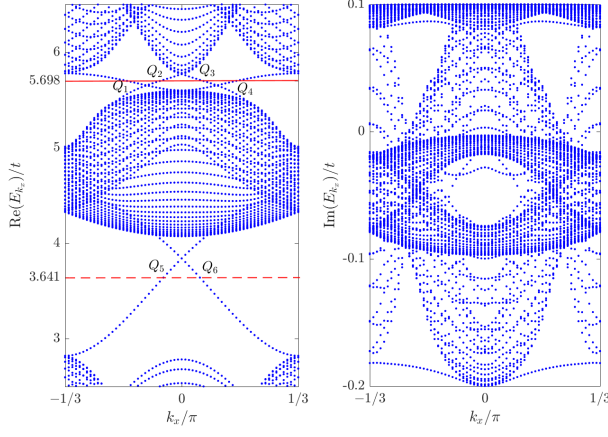


Figure 7: Edge-state spectra with an armchair edge. Left panel: Real edge-state spectra $\text{Re}(E_{k_x})$ (Part of the lower and higher $\text{Re}(E_{k_x})$ are not shown). Right panel: Imaginary edge-state spectra $\text{Im}(E_{k_x})$. The bulk-edge correspondence can be readily seen in the real spectrum. As it shows, there are two pairs of edge modes within the upper bulk gap and a pair of edge modes within the lower bulk gap, corresponding to $C_{\frac{2}{3}} = -2$ and $C_{\frac{1}{3}} = 1$, respectively. Four edge modes, labeled as Q_1 , Q_4 , Q_2 and Q_3 are chosen at $\text{Re}(E_{k_x})=5.698t$ (red solid line) and a pair of edge modes, labeled as Q_5 and Q_6 are chosen at $\text{Re}(E_{k_x})=3.641t$ (red dashed line). In contrast, we cannot observe the bulk-edge correspondence in the imaginary spectrum clearly. Other involved parameter is $N_{\text{armchair}} = 123$, and the number of discrete k_x is 65.

Similarly, energy spectra are plotted at three parameter points mentioned in the previous subsection, shown in Figs. 6(a)-6(f). The left panel shows the real spectra at three chosen parameter points, whereas the right panel corresponds to the imaginary parts. Although there is a certain broadening of the three spectra, the energies are continuous with no obvious band separation. On the contrary, there are distinct band gaps in the real parts. Similar to the imbalanced dissipation case, the topology of this system remains protected by the real gaps [31, 32]. Naturally, the bulk-edge correspondence of this balanced dissipative system can also be directly seen from real edge-state spectra. By choosing the parameter point (η_b, Δ_b) , we plot the associated edge-state spectra in the armchair edge case, shown in Figs. 7(a) and 7(b), respectively.

Figure 7(a) is the real part of edge-state spectrum, in which there are distinct two pairs of edge modes within the upper bulk gap and a pair of edge modes within the bottom bulk gap, corresponding to $C_{\frac{2}{3}} = -2$ and $C_{\frac{1}{3}} = 1$, respectively. In contrast, there are no directly visible bulk-edge correspondence in the imaginary spectrum (see Fig. 7(b)). In order to understand the bulk-edge correspondence adequately, four edge modes, labeled as Q_1 , Q_4 , Q_2 and Q_3 , are chosen at $\text{Re}(E_{k_x})=5.698t$ (red solid

line), and a pair of edge modes, labeled as Q_5 and Q_6 , are chosen at $\text{Re}(E_{k_x})=3.641t$ (red dashed line).

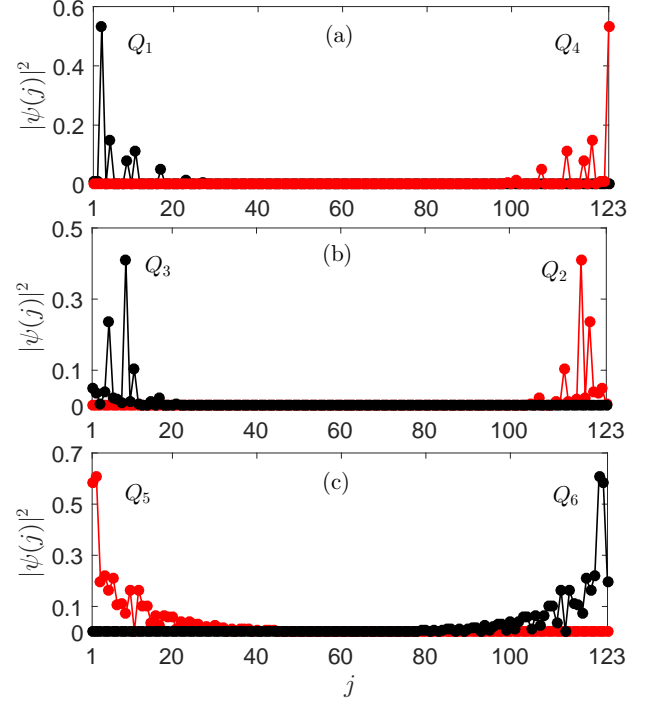


Figure 8: The spatial density distributions of edge modes Q_1 - Q_6 . Edge modes with positive group velocity are shown in red, whereas those with negative group velocity are shown in black, presenting the chiral symmetry. j is the site index.

Figure 8 contains the spatial density distributions of these six chosen edge modes. Similarly, edge modes with positive group velocity are shown in red, whereas those with negative group velocity are shown in black, presenting the chiral symmetry. Then an effective measure is taken to analyze the relationship between the Chern numbers and corresponding edge states, namely, the principle of bulk-edge correspondence [13]. We focus on the edge modes localized at the $j = N_{\text{armchair}}$ side. According to the phase diagram in Fig. 2(a), we know that the edge mode Q_6 carries the Chern number $C = C_{\frac{1}{3}} = 1$, namely $C_1 = 1$. Therefore, the Chern number of edge modes Q_2 and Q_4 , which are opposite to the group velocity of Q_6 , is $C = -1$. Consequently, the middle band has a large Chern number with $C_2 = -1 + (-1) - C_1 = -3$. These analyses are self-consistent with the phase diagrams and the real edge-state spectrum.

V. SUMMARY

To sum up, a non-Hermitian system with an imbalanced dissipation and a balanced dissipation was studied. Our work suggests that the large Chern numbers are robust against the non-Hermitian perturbations. Besides, from the energy spectra and the edge-state spectra, we have known that the associated edge states are protected by the real bulk gaps. In addition, the relationship between the Chern numbers and the spatial density distributions of edge modes are discussed by the principle of the bulk-edge correspondence, which is self-consistent with our phase diagrams and the edge-state spectra.

VI. ACKNOWLEDGE

We thank the discussions with S. Chen and acknowledge the support from NSFC under Grants No. 11835011 and No. 11774316.

-
- [1] M. Z. Hasan and C. L. Kane, Colloquium: Topological insulators, *Rev. Mod. Phys.* **82**, 3045 (2010).
 - [2] X.-L. Qi and S.-C. Zhang, Topological insulators and superconductors, *Rev. Mod. Phys.* **83**, 1057 (2011).
 - [3] G. Harari, M. A. Bandres, Y. Lumer, M. C. Rechtsman, Y. D. Chong, M. Khajavikhan, D. N. Christodoulides, and M. Segev, Topological insulator laser: Theory, *Science*, **359**, 4003 (2018).
 - [4] T. Ozawa, H. M. Price, A. Amo, N. Goldman, M. Hafezi, L. Lu, M. C. Rechtsman, D. Schuster, J. Simon, O. Zilberberg, and I. Carusotto, Topological Photonics, *Rev. Mod. Phys.* **91**, 015006 (2019).
 - [5] J. Dalibard, F. Gerbier, G. Juzeliūnas, and P. Öhberg, Artificial gauge potentials for neutral atoms, *Rev. Mod. Phys.* **83**, 1523 (2011).
 - [6] A. Eckardt, Colloquium: Atomic quantum gases in periodically driven optical lattices, *Rev. Mod. Phys.* **89**, 011004 (2017).
 - [7] N. Cooper, J. Dalibard, and I. Spielman, Topological bands for ultracold atoms, *Rev. Mod. Phys.* **91**, 015005 (2019).
 - [8] D. J. Thouless, M. Kohmoto, M. P. Nightingale, and M. den Nijs, Quantized Hall Conductance in a Two-Dimensional Periodic Potential, *Phys. Rev. Lett.* **49**, 405 (1982).
 - [9] X. G. Wen, Topological orders in rigid states, *Int. J. Mod. Phys. B* **4**, 239 (1990).
 - [10] A. P. Schnyder, S. Ryu, A. Furusaki, and A. W. W. Ludwig, *Phys. Rev. B* **78**, 195125 (2008).
 - [11] C.-K. Chiu, J. C. Y. Teo, A. P. Schnyder, and S. Ryu, Classification of topological quantum matter with symmetries, *Rev. Mod. Phys.* **88**, 035005 (2016).
 - [12] Y. Hatsugai, Chern number and edge states in the integer quantum Hall effect, *Phys. Rev. Lett.* **71**, 3697 (1993).
 - [13] M. S. Rudner, N. H. Lindner, E. Berg, and M. Levin, Anomalous Edge States and the Bulk-Edge Correspondence for Periodically Driven Two-Dimensional Systems, *Phys. Rev. X* **3**, 031005 (2013).
 - [14] W. P. Su, J. R. Schrieffer, and A. J. Heeger, Solitons in Polyacetylene, *Phys. Rev. Lett.* **42**, 1698 (1979).
 - [15] F. D. M. Haldane, Model for a Quantum Hall Effect without Landau Levels: Condensed-Matter Realization of the "Parity Anomaly", *Phys. Rev. Lett.* **61**, 2015 (1988).
 - [16] D. R. Hofstadter, Energy levels and wave functions of Bloch electrons in rational and irrational magnetic fields, *Phys. Rev. B* **14**, 2239 (1976).
 - [17] C. L. Kane and E. J. Mele, Quantum Spin Hall Effect in Graphene, *Phys. Rev. Lett.* **95**, 226801 (2005); Z_2 Topological Order and the Quantum Spin Hall Effect, *ibid.*, **95**, 146802 (2005).
 - [18] C.-Z. Chang, J. Zhang, X. Feng, J. Shen, Z. Zhang, M. Guo, K. Li, Y. Ou, P. Wei, L.-L. Wang, Z.-Q. Ji, Y. Feng, S. Li, X. Chen, J. Jia, X. Dai, Z. Fang, S.-C. Zhang, K. He, Y. Wang, L. Lu, X.-C. Ma, and Q.-K. Xue, Experimental observation of the quantum anomalous Hall effect in a magnetic topological insulator, *Science* **340**, 167 (2013).
 - [19] C.-Z. Chang, W. Zhao, D. Y. Kim, H. Zhang, B. A. Assaf, D. Heiman, S.-C. Zhang, C. Liu, M. H. W. Chan, J. S. Moodera, High-precision realization of robust quantum anomalous Hall state in a hard ferromagnetic topological insulator, *Nat. Mater.* **14**, 473 (2015).
 - [20] Y. Deng, Y. Yu, M. Z. Shi, Z. Guo, Z. Xu, J. Wang, X. H. Chen, and Y. Zhang, Quantum anomalous Hall effect in intrinsic magnetic topological insulator MnBi_2Te_4 , *Science*, **367**, 895 (2020).
 - [21] A. Kitaev, Unpaired Majorana fermions in quantum wires, *Phys. Usp.* **44**, 131 (2002).
 - [22] A. Kitaev, Periodic table for topological insulators and superconductors, *AIP Conf. Proc.*, **1134**, 22 (2009).
 - [23] C. Nayak, S. H. Simon, A. Stern, M. Freedman, and S. Das Sarma, Non-Abelian anyons and topological quantum computation, *Rev. Mod. Phys.* **80**, 1083 (2008).
 - [24] V. V. Konotop, J. Wang, and D. A. Zezyulin, Nonlinear waves in \mathcal{PT} -symmetric systems, *Rev. Mod. Phys.* **88**, 035002 (2016).
 - [25] R. El-Ganainy, K. G. Makris, M. Khajavikhan, Z. H. Musslimani, S. Rotter, and D. N. Christodoulides, Non-Hermitian physics and \mathcal{PT} symmetry, *Nat. Phys.* **14**, 11 (2018).
 - [26] C. M. Bender and S. Boettcher, Real spectra in non-Hermitian Hamiltonians having \mathcal{PT} symmetry, *Phys. Rev. Lett.* **80**, 5243 (1998).
 - [27] C. M. Bender, Making sense of non-Hermitian Hamiltonians, *Rep. Prog. Phys.* **70**, 947 (2007).
 - [28] K. G. Makris, R. El-Ganainy, D. N. Christodoulides, and Z. H. Musslimani, Beam Dynamics in \mathcal{PT} Symmetric Optical Lattices, *Phys. Rev. Lett.* **100**, 103904 (2008).
 - [29] S. Longhi, Bloch Oscillations in Complex Crystals with \mathcal{PT} Symmetry, *Phys. Rev. Lett.* **103**, 123601 (2009).
 - [30] S. Klaiman, U. Günther, and N. Moiseyev, Visualization of Branch Points in \mathcal{PT} -Symmetric Waveguides, *Phys. Rev. Lett.* **101**, 080402 (2008).
 - [31] K. Esaki, M. Sato, K. Hasebe, and M. Kohmoto, Edge states and topological phases in non-Hermitian systems, *Phys. Rev. B* **84**, 205128 (2011).
 - [32] H. Menke and M. M. Hirschmann, Topological quantum wires with balanced gain and loss, *Phys. Rev. B* **95**, 174506 (2017).
 - [33] D. Leykam, K. Y. Bliokh, C. Huang, Y. D. Chong, and F.

- Nori, Edge Modes, Degeneracies, and Topological Numbers in Non-Hermitian Systems, *Phys. Rev. Lett.* **118**, 040401 (2017).
- [34] S. Lieu, Topological phases in the non-Hermitian Su-Schrieffer-Heeger model, *Phys. Rev. B* **97**, 045106 (2018).
- [35] M. S. Rudner and L. S. Levitov, Topological Transition in a Non-Hermitian Quantum Walk, *Phys. Rev. Lett.* **102**, 065703 (2009).
- [36] C. Li, X. Z. Zhang, G. Zhang, and Z. Song, Topological phases in a Kitaev chain with imbalanced pairing, *Phys. Rev. B* **97**, 115436 (2018).
- [37] T. E. Lee, Anomalous Edge State in a Non-Hermitian Lattice, *Phys. Rev. Lett.* **116**, 133903 (2016).
- [38] K. Kawabata, K. Shiozaki, M. Ueda, and M. Sato, Symmetry and Topology in Non-Hermitian Physics, *Phys. Rev. X* **9**, 041015 (2019).
- [39] D. C. Brody, Biorthogonal quantum mechanics, *J. Phys. A: Math. Theor.* **47**, 035305 (2013).
- [40] S. Yao and Z. Wang, Edge States and Topological Invariants of Non-Hermitian Systems, *Phys. Rev. Lett.* **121**, 086803 (2018); S. Yao, F. Song, and Z. Wang, Non-Hermitian Chern bands, *ibid.*, **121**, 136802 (2018).
- [41] K. Yokomizo and S. Murakami, Non-Bloch Band Theory of Non-Hermitian Systems, *Phys. Rev. Lett.* **123**, 066404 (2019).
- [42] Z. Gong, Y. Ashida, K. Kawabata, K. Takasan, S. Higashikawa, and M. Ueda, Topological Phases of Non-Hermitian Systems, *Phys. Rev. X* **8**, 031079 (2018).
- [43] K. Kawabata, S. Higashikawa, Z. Gong, Y. Ashida, and M. Ueda, Topological unification of time-reversal and particle-hole symmetries in non-Hermitian physics, *Nat. Commun.* **10**, 297 (2019).
- [44] K. Kawabata, K. Shiozaki, and M. Ueda, Anomalous helical edge states in a non-Hermitian Chern insulator, *Phys. Rev. B* **98**, 165148 (2018).
- [45] S.-D. Liang and G.-Y. Huang, Topological Invariance and Global Berry Phase in Non-Hermitian Systems, *Phys. Rev. A* **87**, 012118 (2013).
- [46] H. Shen, B. Zhen, and L. Fu, Topological Band Theory for Non-Hermitian Hamiltonians, *Phys. Rev. Lett.* **120**, 146402 (2018).
- [47] F. K. Kunst, E. Edvardsson, J. C. Budich, and E. J. Bergholtz, Biorthogonal Bulk-Boundary Correspondence in Non-Hermitian Systems, *Phys. Rev. Lett.* **121**, 026808 (2018).
- [48] K. Kawabata, K. Shiozaki, and M. Ueda, Anomalous helical edge states in a non-Hermitian Chern insulator, *Phys. Rev. B* **98**, 165148 (2018).
- [49] L. Jin and Z. Song, Bulk-boundary correspondence in a non-Hermitian system in one dimension with chiral inversion symmetry, *Phys. Rev. B* **99**, 081103(R) (2019).
- [50] C. H. Lee, L. Li, and J. Gong, Hybrid Higher-Order Skin-Topological Modes in Nonreciprocal Systems, *Phys. Rev. Lett.* **123**, 016805 (2019).
- [51] T. Liu, Y.-R. Zhang, Q. Ai, Z. Gong, K. Kawabata, M. Ueda, and F. Nori, Second-Order Topological Phases in Non-Hermitian Systems, *Phys. Rev. Lett.* **122**, 076801 (2019).
- [52] K. Kawabata, N. Okuma, and M. Sato, Non-Bloch band theory of non-Hermitian Hamiltonians in the symplectic class, *Phys. Rev. B* **101**, 195147 (2020).
- [53] E. J. Bergholtz, J. C. Budich, and F. K. Kunst, Exceptional Topology of non-Hermitian Systems, *arXiv*: 1912.10048.
- [54] F. K. Kunst and V. Dwivedi, Non-Hermitian systems and topology: A transfer-matrix perspective, *Phys. Rev. X* **9**, 245116 (2019).
- [55] N. Okuma, K. Kawabata, K. Shiozaki, and M. Sato, Topological Origin of Non-Hermitian Skin Effects, *Phys. Rev. Lett.* **124**, 086801 (2019).
- [56] L. Zhou, Dynamical characterization of non-Hermitian Floquet topological phases in one dimension, *Phys. Rev. B* **100**, 184314 (2019).
- [57] X. Zhang and J. Gong, Non-Hermitian Floquet topological phases: Exceptional points, coalescent edge modes, and the skin effect, *Phys. Rev. B* **101**, 045415 (2020).
- [58] J. M. Zeuner, M. C. Rechtsman, Y. Plotnik, Y. Lumer, S. Nolte, M. S. Rudner, M. Segev, and A. Szameit, Observation of a Topological Transition in the Bulk of a Non-Hermitian System, *Phys. Rev. Lett.* **115**, 040402 (2015).
- [59] C. Poli, M. Bellec, U. Kuhl, F. Mortessagne, and H. Schomerus, Selective enhancement of topologically induced interface states in a dielectric resonator chain, *Nat. Commun.* **6**, 6710 (2015).
- [60] L. Xiao, X. Zhan, Z. H. Bian, K. K. Wang, X. Zhang, X. P. Wang, J. Li, K. Mochizuki, D. Kim, N. Kawakami, W. Yi, H. Obuse, B. C. Sanders, and P. Xue, Observation of topological edge states in parity-time-symmetric quantum walks, *Nat. Phys.* **13**, 1117 (2017).
- [61] S. Weimann, M. Kremer, Y. Plotnik, Y. Lumer, S. Nolte, K. G. Makris, M. Segev, M. C. Rechtsman, and A. Szameit, Topological protected bound states in photonic parity-time-symmetric crystals, *Nat. Mater.* **16**, 433 (2017).
- [62] M. Parto, S. Wittek, H. Hodaei, G. Harari, M. A. Bandres, J. Ren, M. C. Rechtsman, M. Segev, D. N. Christodoulides, and M. Khajavikhan, Complex Edge-State Phase Transitions in 1D Topological Laser Arrays, *Phys. Rev. Lett.* **120**, 113901 (2018).
- [63] H. Zhao, P. Miao, M. H. Teimourpour, S. Malzard, R. El-Ganainy, H. Schomerus, and L. Feng, Topological hybrid silicon microlasers, *Nat. Commun.* **9**, 981 (2018).
- [64] P. St-Jean, V. Goblot, E. Galopin, A. Lemaître, T. Ozawa, L. Le Gratiet, I. Sagnes, J. Bloch, and A. Amo, Lasing in topological edge states of a one-dimensional lattice, *Nat. Photon.* **11**, 651 (2017).
- [65] H. Zhao, X. Qiao, T. Wu, B. Midya, S. Longhi, and L. Feng, Non-Hermitian topological light steering, *Science* **365**, 1163 (2019).
- [66] M. A. Bandres, S. Wittek, G. Harari, M. Parto, J. Ren, M. Segev, D. Christodoulides, and M. Khajavikhan, Topological insulator laser: Experiments, *Science* **359**, eaar4005 (2018).
- [67] T. Andrijauskas, E. Anisimovas, M. Račiūnas, A. Mekys, V. Kudriašov, I. B. Spielman, and G. Juzeliūnas, Three-level Haldane-like model on a dice optical lattice, *Phys. Rev. A* **92**, 033617 (2015).
- [68] S. Cheng, H. Yin, Z. Lu, C. He, P. Wang, and G. Xianlong, Predicting large-Chern-number phases in a shaken optical dice lattice, *Phys. Rev. A* **101**, 043620 (2020).
- [69] B. Dey, P. Kapri, O. Pal, and T. K. Ghosh, Unconventional phases in a Haldane model of dice lattice, *Phys. Rev. B* **101**, 235406 (2020).
- [70] B. Sutherland, Localization of electronic wave functions due to local topology, *Phys. Rev. B* **34**, 5208 (1986).
- [71] J. Vidal, P. Butaud, B. Doucot, and R. Mosseri, Disorder and interactions in Aharonov-Bohm cages, *Phys. Rev. B* **64**, 155306 (2001).

- [72] M. Rizzi, V. Cataudella, and R. Fazio, Phase diagram of the Bose-Hubbard model with T3 symmetry, *Phys. Rev. B* **73**, 144511 (2006).
- [73] A. A. Burkov and E. Demler, Vortex-Peierls States in Optical Lattices, *Phys. Rev. Lett.* **96**, 180406 (2006).
- [74] G. Möller and N. R. Cooper, Correlated Phases of Bosons in the Flat Lowest Band of the Dice Lattice, *Phys. Rev. Lett.* **108**, 045306 (2012).
- [75] R. Barnett, G. R. Boyd, and V. Galitski, SU(3) Spin-orbit coupling in systems of ultracold atoms, *Phys. Rev. Lett.* **109**, 235308 (2012).
- [76] H. Georgi, *Lie Algebras In Particle Physics: from Isospin To Unified Theories* (Benjamin/Cummings, Reading, MA, 1982).